Projection Method for Incompressible Flow

Knut Sverdrup

Abstract

In this report, we discuss computational methods for solving the incompressible Navier-Stokes equations in the two-dimensional test case of a lid-driven cavity. For Newtonian fluids, we demonstrate the implementation of a fractional-step projection method for solving the transient problem with high Reynolds numbers, and show that the system converges to the steady-state solution previously documented in the literature. Additionaly, we discuss the case of Reynolds number zero in Bingham plastic fluids, and how the steady-state solution can be computed through the SIMPLE algorithm when regularization is employed to deal with the singularity in apparent viscosity of such fluids.

1. Introduction

In physics, few equations span as wide a range of applications as the Navier-Stokes equations of fluid dynamics. They govern the motion of viscous fluids in a continuum framework, and as such have applications in *e.g.* climate modelling [1,2], aerodynamics [3–5], medicinal research [6,7] and petroleum engineering [8–11], to name a few. Named after Claude Navier and George Stokes for their major contributions [12,13] to its formulation in the first half of the nineteenth century, the equations have constituted a major field of research in their own right since their formulation, and continue to do so today. Apart from their numerous applications, the equations are fundamentally interesting from a mathematical point of view. In fact, (dis-)proving the existence and uniqueness of their solutions is one of the seven Millenium prize problems [14] for which a prize of one million US dollars is associated.

The generalized Navier-Stokes equations are based on the conservation of mass through the continuity equation,

$$\partial_t \rho + \nabla \cdot (\rho \boldsymbol{u}) = 0\,, \tag{1}$$

in addition to conservation of momentum as given by the Cauchy momentum equation

$$\rho\left(\partial_t \boldsymbol{u} + \boldsymbol{u}\cdot\nabla\boldsymbol{u}\right) = -\nabla p + \nabla\cdot\boldsymbol{\tau} + \boldsymbol{f}\,. \tag{2}$$

Here, we have introduced the primitive variables density ρ, velocity $\boldsymbol{u}$ and pressure p, in addition to the deviatoric stress tensor $\boldsymbol{\tau}$. The vector $\boldsymbol{f}$ accounts for external body sources such as gravity acting on the fluid, and shall henceforth be disregarded. The Navier-Stokes equations are an extension of Eqns. (1) and (2) derived under the assumptions that the stress tensor $\boldsymbol{\tau}$ is a linear function of the strain tensor $\dot{\boldsymbol{\gamma}} = \nabla\boldsymbol{u} + (\nabla\boldsymbol{u})^T$, that $\nabla\cdot\boldsymbol{\tau} = 0$ for fluids at rest, and that the fluid is isotropoc. Given these assumptions, Eq. (2) can be rewritten

$$\rho\left(\partial_t \boldsymbol{u} + \boldsymbol{u}\cdot\nabla\boldsymbol{u}\right) = -\nabla p + \nabla\cdot(\mu\dot{\boldsymbol{\gamma}}) + \nabla\left(\lambda\nabla\cdot\boldsymbol{u}\right) \tag{3}$$

where μ and λ are the first and second coefficients of viscosity, respectively. Fluids which obey the Navier-Stokes equations as given by Eqns. (1) and (3) are labelled Newtonian fluids. The second coefficient of viscosity, λ, is related to bulk viscosity and disappears for incompressible flow, which we restrict ourselves to in this project. Consequently, we shall simply refer to μ as the viscosity of the fluid in the following.

When the density ρ is constant within each control volume of the fluid, the flow is said to be isochoric or incompressible. A vast amount of cases in continuum mechanics relate to incompressible flow, and several simplifications arise in the description of the fluid. Firstly, Eq. (1) reduces to the incompressibility constraint

$$\nabla\cdot\boldsymbol{u} = 0\,. \tag{4}$$

Secondly, the viscosity μ is constant for incompressible flow. Consequently, Eq. (3) simplifies to

$$\rho\left(\partial_t \boldsymbol{u} + \boldsymbol{u}\cdot\nabla\boldsymbol{u}\right) = -\nabla p + \mu\nabla^2\boldsymbol{u}\,, \qquad (5)$$

where we have used the fact that $\nabla\cdot\dot{\boldsymbol{\gamma}} = \nabla^2\boldsymbol{u}$ for incompressible flow. Eqns. (4) and (5) make up the incompressible Navier-Stokes equations for incompressible flow.

In order to nondimensionalize our system of equations, we move to dimensionless variables such that $\boldsymbol{u} \to \frac{1}{a}\boldsymbol{u}$, $\partial_t \to \frac{L}{a}\partial_t$ and $\nabla \to L\nabla$, where L is the length of the system under consideration and a is the maximum absolute value of the velocity. Applying these changes to Eq. (5) and multiplying through by $L/(\rho a^2)$ gives the dimensionless equation

$$\partial_t \boldsymbol{u} + \boldsymbol{u}\cdot\nabla\boldsymbol{u} = -\frac{1}{\rho a^2}\nabla p + \frac{1}{\mathrm{Re}}\nabla^2\boldsymbol{u}\,. \qquad (6)$$

Here, $\mathrm{Re} = \rho a L/\mu$ is the Reynolds number of the flow, which equals the ratio of intertial forces to viscous ones. Note that the pressure is still measured in physical units, as we wish to utilize different scalings depending on the Reynolds number. Low Reynolds numbers correspond to laminar flow, where the viscous forces are dominant. In this case, we let $p \to \frac{\mathrm{Re}}{\rho a^2}p$, so that Eq. (6) becomes

$$\mathrm{Re}\left(\partial_t \boldsymbol{u} + \boldsymbol{u}\cdot\nabla\boldsymbol{u}\right) = -\nabla p + \nabla^2\boldsymbol{u}\,. \qquad (7)$$

High Reynolds numbers, on the other hand, correspond to turbulent flow with the most important contributions arising from the intertial forces. We then let $p \to \frac{1}{\rho a^2}p$, yielding the alternative formulation

$$\partial_t \boldsymbol{u} + \boldsymbol{u}\cdot\nabla\boldsymbol{u} = -\nabla p + \frac{1}{\mathrm{Re}}\nabla^2\boldsymbol{u}\,. \qquad (8)$$

In our implementation of fractional step projection methods for incompresible flow of Newtonian fluids, Eq. (8) is the formulation of interest. When discussing creeping flow for Bingham plastic fluids, however, we return to (a variant of) Eq. (7).

Several models exist to describe different types of Non-Newtonian fluids, each characterized by the way the stress $\tau = \sqrt{\frac{1}{2}\sum \boldsymbol{\tau}_{i,j}^2}$ depends on the strain rate $\dot{\gamma} = \sqrt{\frac{1}{2}\sum \dot{\boldsymbol{\gamma}}_{i,j}^2}$. The interesting variable is the apparent viscosity $\eta = \tau/\dot{\gamma}$. For Newtonian fluids, as we have already seen, the relationship is linear, with slope $\eta = \mu$. Non-Newtonian fluids include dilatants (shear-thickening, $\partial\eta/\partial\dot{\gamma} > 0$) and pseudoplastics (shear-thinning, $\partial\eta/\partial\dot{\gamma} < 0$), but in this project we restrict ourselves to the relatively simple case of Bingham plastics. Figure 1 illustrates the different types of fluids.

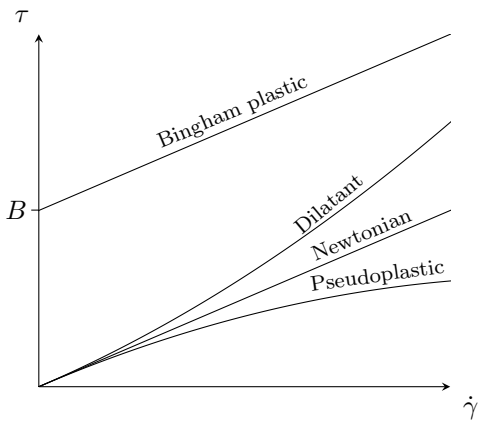

Figure 1: Classification of fluids based on apparent viscosity.

Bingham plastic fluids, named after Eugene Cook Bingham for his investigation into them in 1916 [15], have a threshold stress τ_0, below which they do not yield to applied forces. For the nondimensionalized stress tensor, the yield stress corresponds to the dimensionless Bingham number $B = \tau_0 L/(\mu a)$. In other words, the strain rate is zero unless a stress higher than that characteristic stress is applied. Physically, this means that they behave as solids for small stresses, something which leads to interesting behaviour such as non-flat surfaces at rest. Regions where the flow is such that $\tau < B$ are also known as unyielded regions. The relationship between stress and shear rate for Bingham plastics is therefore

$$\dot{\gamma} = \begin{cases} 0\,, & \tau \le B \\ \tau - B\,, & \tau > B \end{cases}\,, \qquad (9)$$

from which it is evident that the apparent viscosity

$$\eta = \frac{B}{\dot{\gamma}} + 1\,, \qquad (10)$$

and as such has a singularity for $\dot{\gamma} = 0$.

As a test framework for our numerical schemes, we apply them to the so-called lid-driven cavity problem. The problem has served as a benchmark test for viscous, incompressible fluid flow for decades, and reference solutions are readily available, notably those produced by Ghia *et al.* in 1982 through the vorticity-strem function formulation and multigrid methods [16]. This test case is fairly simple, and consists of a square domain in

2D with sides of length L. At all sides, both solid-wall and no-slip boundary conditions are applied, so that the component of $\boldsymbol{u} = (u, v)^T$ normal to the wall is zero on the whole boundary, while the tangential component equals the velocity of wall. In the lid-driven cavity test, all walls are stationary except the top one (the "lid"), which moves with constant speed a. Figure 2 exhibits the test case schematically.

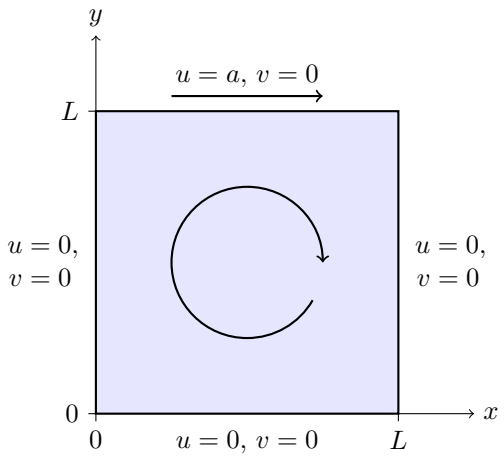

Figure 2: Lid-driven cavity test case.

In Section 2, the numerical methods employed to solve the incompressible Navier-Stokes equations for Newtonian fluids in the lid-driven cavity are explained, in addition to the extensions needed for creeping flow of Bingham plastics. Section 3 contains our results, which are the basis of the discussion following in Section 4. Section 5 concludes the report.

2. Numerical methods

2.1. Newtonian fluid

2.1.1. Projection method

In order to solve the transient problem given by Eqns. (8) and (4), we implement a fractional-step projection method following section 10.3 of Oleg Zikanov's *Essential Computational Fluid Dynamics*[17]. The original projection method for Navier-Stokes equations was invented by Chorin in 1968[18], and the essence is still the same in modern variants. It is an operator splitting approach, in which, for each time step, one first performs an intermediate time step while ignoring the pressure forces, and then ignores the viscous forces in the second time step. Temporal discretization of Eq.(8) is done explicitly for the nonlinear term and implicitly for the linear ones, yielding the two equations

$$\frac{\tilde{\boldsymbol{u}}^{n+1} - \boldsymbol{u}^n}{\Delta t} + \boldsymbol{u}^n \cdot \nabla \boldsymbol{u}^n - \frac{1}{\mathrm{Re}} \nabla^2 \tilde{\boldsymbol{u}}^{n+1} = 0\,, \quad (11)$$

$$\frac{\boldsymbol{u}^{n+1} - \tilde{\boldsymbol{u}}^{n+1}}{\Delta t} + \nabla p^{n+1} = 0\,, \quad (12)$$

which reduce to the discrete version of Eq. (8) when added together. Here, we have introduced the notation $\boldsymbol{u}^n = \boldsymbol{u}(n\Delta t)$, in addition to denoting by $\tilde{\boldsymbol{u}}^{n+1}$ the velocity at the intermediate time step. It is particularly important to utilize the implicit temporal discretization for flows with low Reynolds numbers and for meshes that are stretched near boundaries, since otherwise the numerical viscous stability restriction becomes severe in these cases.

Given a suitable spatial discretization scheme, Eq. (11) is straightforward to solve since there is one known ($\boldsymbol{u}^n$) and one unknown ($\tilde{\boldsymbol{u}}^{n+1}$) quantity. The second step, however, has two unknowns. This problem is solved by taking the divergence of Eq.(12) and enforcing $\nabla \cdot \boldsymbol{u}^{n+1} = 0$, leading to a Poisson equation for the pressure:

$$\nabla^2 p^{n+1} = \frac{1}{\Delta t} \nabla \cdot \tilde{\boldsymbol{u}}^{n+1}\,. \quad (13)$$

By doing so, the intermediate, unphysical velocity, which was computed without enforcing incompressibility, is projected onto the space of vector fields satistfying Eq. (4). Note that the boundary conditions are also affected by taking the divergence, as by doing so the Dirichlet conditions are transformed to Neumann type.

The velocity at time t^{n+1} can finally be updated by rearranging Eq. (12) to read

$$\boldsymbol{u}^{n+1} = \tilde{\boldsymbol{u}}^{n+1} + \Delta t \nabla p^{n+1}\,. \quad (14)$$

2.1.2. Finite volumes

Spatial discretization is done through finite volumes with a staggered grid, *i.e.* a grid where the three primitive variables are evaluated at different points. The need for a staggered grid is due to the relationship between pressure and velocity. On a regular grid, a checkerboard pattern occurs in their dependencies upon each other, leading to decoupling and thus spurious pressure instabilities. Our domain is split into N equal subdomains for pressure in each spatial direction, leading to a total of

N^2 subdomains of area Δx^2, where $\Delta x = 1/N$ (we employ the same grid spacing in both directions). In the centre of each of these squares, the pressure is evaluated, while the x- and y-components of velocity are evaluated on their vertical and horizontal borders, respectively. Consequently, the control volumes for the first and second components of the momentum balance equations in the finite volume method are shifted by $\frac{1}{2}\Delta x$ compared to the control volumes used for the Poisson equation for pressure. The staggered grid with shifted control volumes is illustrated in Figure 3.

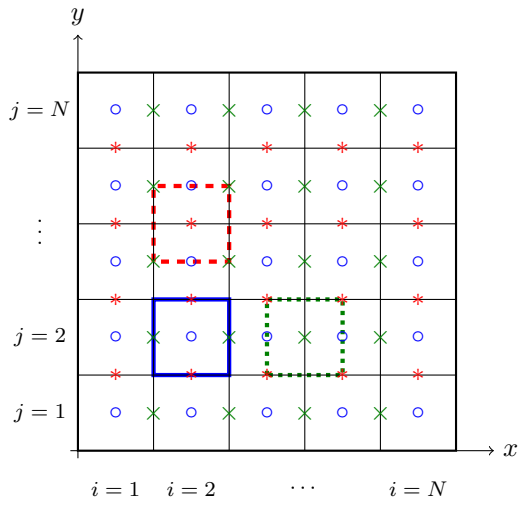

Figure 3: Spatial discretization of the square domain with a staggered grid. At the different points, the primitive variables are evaluated: ∘ p, × u, ∗ v. Examples of control volumes for pressure ($i = 2$, $j = 2$), x-velocity ($i = 3.5$, $j = 2$) and y-velocity ($i = 2$,$j = 2.5$) are also shown with corresponding colors. In this example, $N = 5$.

We denote by $\Omega_{i,j}$ the control volume centred at $(x_i, y_j) = (i\Delta x - 1/2, j\Delta x - 1/2)$. In integral form over a control volume centred at a u-point, the first component of Eq. (11) reads

$$\int_{\Omega_{i+\frac{1}{2},j}} \tilde{u}^{n+1}\mathrm{d}V - \frac{\Delta t}{\mathrm{Re}}\int_{\Omega_{i+\frac{1}{2},j}} \nabla^2\tilde{u}^{n+1}\mathrm{d}V = \int_{\Omega_{i+\frac{1}{2},j}} u^n\mathrm{d}V + \Delta t\int_{\Omega_{i+\frac{1}{2},j}} (u^n\partial_x u^n + v^n\partial_y u^n)\mathrm{d}V\,. \tag{15}$$

We approximate the first term on each side of the equation by the two-dimensional midpoint rule, *i.e.*

$$\int_{\Omega_{i+\frac{1}{2},j}} \tilde{u}^{n+1}\mathrm{d}V \approx \tilde{u}^{n+1}_{i+\frac{1}{2},j}(\Delta x)^2\,, \tag{16}$$

and similar for u^n. Derivatives are approximated by central differences, and when evaluation of a variable is necessary at a point where it is not defined, the mean value of the nearest neighbours to the point is taken instead. Thus, the integral in the term with the Laplacian becomes

$$\int_{\Omega_{i+\frac{1}{2},j}} \nabla^2\tilde{u}^{n+1}\mathrm{d}V = \int_{\partial\Omega_{i+\frac{1}{2},j}} \partial_n\tilde{u}^{n+1}\mathrm{d}S \approx \tilde{u}^{n+1}_{i+\frac{3}{2},j} + \tilde{u}^{n+1}_{i+\frac{3}{2},j} + \tilde{u}^{n+1}_{i+\frac{3}{2},j} + \tilde{u}^{n+1}_{i+\frac{3}{2},j} - 4\tilde{u}^{n+1}_{i+\frac{3}{2},j}\,, \tag{17}$$

while the integrals in the nonlinear term are approximated as

$$\int_{\Omega_{i+\frac{1}{2},j}} u^n\partial_x u^n\mathrm{d}V \approx u^n_{i+\frac{1}{2},j}\frac{1}{2}(u^n_{i+\frac{3}{2},j} - u^n_{i-\frac{1}{2},j})\Delta x\,, \tag{18}$$

$$\int_{\Omega_{i+\frac{1}{2},j}} v^n\partial_y u^n\mathrm{d}V \approx \frac{1}{2}(u^n_{i+\frac{1}{2},j+1} - u^n_{i+\frac{1}{2},j-1})\Delta x \times\frac{1}{4}(v^n_{i+1,j+\frac{1}{2}} + v^n_{i+1,j-\frac{1}{2}} + v^n_{i+1,j+\frac{1}{2}} + v^n_{i+1,j-\frac{1}{2}})\,. \tag{19}$$

By substituting the approximations in Eqns. (16) - (19) in Eq. (15), we arrive at a matrix equation of the form

$$A_{uv}\tilde{\mathbf{u}} = \mathbf{f}_u + \mathbf{b}_u\,, \tag{20}$$

where A_{uv} is an $N(N-1)\times N(N-1)$ matrix, $\tilde{\mathbf{u}}$ is a vector containing the discrete values of $\tilde{u}^{n+1}$ at each point and $\mathbf{f}_u$ is a load vector depending only on values of $\mathbf{u}$ and $\mathbf{v}$ at the previous time step. [1] The vector $\mathbf{b}_u$ takes into consideration the boundary conditions, and will be treated shortly. The matrix is a sparse block tridiagonal matrix of the form

[1] Note that bold symbols in italics refer to physical variables such as $\boldsymbol{u} = (u, v)^T$, while roman bold symbols are vectors of discrete values, *e.g.* $\mathbf{u} = \{u_{i+\frac{1}{2},j}\}$ for $i \in \{1, 2, \ldots, N-1\}$, $j \in \{1, 2, \ldots, N\}$.

$$A_{uv} = \begin{pmatrix} I-\alpha B & -\alpha I & & \\ -\alpha I & I-\alpha B & -\alpha I & \\ & & \ddots & \\ & & -\alpha I & I-\alpha B \end{pmatrix},$$

where $\alpha = \frac{\Delta t}{\mathrm{Re}(\Delta x)^2}$, I is the identity matrix and

$$B = \begin{pmatrix} -4 & 1 & & \\ 1 & -4 & 1 & \\ & & \ddots & \\ & & 1 & -4 \end{pmatrix}.$$

By the exact same procedure for the second component of Eq. (11), using control volumes $\Omega_{i,j+\frac{1}{2}}$, one arrives at a similar equation for the intermediate y-velocities:

$$A_{uv}\tilde{\mathbf{v}} = \mathbf{f}_v + \mathbf{b}_v\,, \tag{21}$$

By comparison, the spatial discretization of Eq. (13) is straightforward. In discrete form over a control volume, it reads

$$\int_{\Omega_{i,j}} \nabla^2 p^{n+1} \mathrm{d}V = \frac{1}{\Delta t}\int_{\Omega_{i,j}} \nabla\cdot\tilde{\boldsymbol{u}}^{n+1}\mathrm{d}V\,. \tag{22}$$

We discretize the pressure term as

$$\begin{aligned}\int_{\Omega_{i,j}} \nabla^2 p^{n+1}\mathrm{d}V &= \int_{\partial\Omega_{i,j}} \nabla p^{n+1}\cdot\mathrm{d}\boldsymbol{S}\\ &\approx p^{n+1}_{i+1,j} + p^{n+1}_{i,j-1} + p^{n+1}_{i-1,j} + p^{n+1}_{i,j+1} - 4p^{n+1}_{i,j}\,,\end{aligned} \tag{23}$$

while the term containing the intermediate velocity becomes

$$\begin{aligned}\int_{\Omega_{i,j}} \nabla\cdot\tilde{\boldsymbol{u}}^{n+1}\mathrm{d}V &= \int_{\partial\Omega_{i,j}} \tilde{\boldsymbol{u}}^{n+1}\cdot\mathrm{d}\boldsymbol{S}\\ &\approx(\tilde{u}^{n+1}_{i+\frac{1}{2},j} - \tilde{u}^{n+1}_{i-\frac{1}{2},j} + \tilde{v}^{n+1}_{i,j+\frac{1}{2}} - \tilde{v}^{n+1}_{i,j-\frac{1}{2}})\Delta x\,.\end{aligned} \tag{24}$$

We thus end up with a system of linear equations:

$$A_p\mathbf{p} = \mathbf{f}_p + \mathbf{b}_p\,. \tag{25}$$

In this case, there are N^2 variables and unknowns, and the matrix is given by

$$A_p = \begin{pmatrix} B & I & & \\ I & B & I & \\ & & \ddots & \\ & & I & B \end{pmatrix}.$$

2.1.3. Boundary conditions

Special consideration must be taken near the boundaries of the domain. The update formula for an x-momentum control volume requires information taken from the four nearest x-momentum control volumes (north, east, south and west) in addition to the four nearest y-momentum control volumes (northeast, southeast, southwest and northwest). Upon investigation of Figure 3, it is evident that we then need ghost cells for $\tilde{u}$ at $i = 1/2$, $i = N + 1/2$, $j = 0$ and $j = N + 1$. The first two are given immediately by the Dirichlet conditions (no-slip, solid wall), while the latter are computed using interpolation.

$$\begin{aligned}\tilde{u}^n_{\frac{1}{2},j} &= 0\,, & \tilde{u}^n_{N+\frac{1}{2},j} &= 0\,,\\ \tilde{u}^n_{i+\frac{1}{2},0} &= -\tilde{u}^n_{i+\frac{1}{2},1}\,, & \tilde{u}^n_{i+\frac{1}{2},N+1} &= 2a - \tilde{u}^n_{i+\frac{1}{2},N}\,.\end{aligned} \tag{26}$$

Utilizing the same technique for $\tilde{v}$, we have

$$\begin{aligned}\tilde{v}^n_{i,\frac{1}{2}} &= 0\,, & \tilde{v}^n_{i,N+\frac{1}{2}} &= 0\,,\\ \tilde{v}^n_{0,j+\frac{1}{2}} &= -\tilde{v}^n_{1,j+\frac{1}{2}}\,, & \tilde{v}^n_{N+1,j+\frac{1}{2}} &= -\tilde{v}^n_{N,j+\frac{1}{2}}\,.\end{aligned} \tag{27}$$

The boundary condiions for p are less obvious, and have been subject to debate in the literature[19]. As there are no physical boundary conditions on p, one could take the inner product of Eq. (8) with either the unit normal or unit tangent at the boundary, and retrieve equally feasile boundary conditions. In general, the former is preferred by most people, since the condition relates naturally to the projection operator. Requiring that the space of divergence-free vector fields is orthogonal to the space of irrotational vector fields results in the boundary condition $\boldsymbol{u}^{n+1}\cdot\boldsymbol{n} = 0$. Taking the inner product of Eq. (12) with $\boldsymbol{n}$ thus gives $\partial_n p = 0$ on the domain border. Our boundary conditions for the pressure are then

$$\begin{aligned}p^{n+1}_{0,j} &= p^{n+1}_{1,j}\,, & p^{n+1}_{i,0} &= p^{n+1}_{i,1}\,,\\ p^{n+1}_{N+1,j} &= p^{n+1}_{N,j}\,, & p^{n+1}_{i,N+1} &= p^{n+1}_{i,N}\,.\end{aligned} \tag{28}$$

2.1.4. Eigen for systems of equations

Each of the linear systems in Eqns. (20), (21) and (25) are solved using a C++ template library

for linear algebra called Eigen[20]. Since the matrices are sparse, we exploit the special sparse datastructures available in Eigen, and solve the systems using a simplicial Cholesky factorization (LDL^T). The choice of factorization is for efficiency, and can be used since the sparse matrics are self-adjoint and positive definite.

2.1.5. Stability and convergence to steady-state

An important question in any time-marching scheme for PDEs is the restriction on the time step Δt necessary to achieve stability. For a nonlinear scheme such as the one employed, analytical stability restrictions are not available to the best knowledge of the author, but it is still possible to gather some insights from investigating the scheme. The restrictions on Δt are dependent on $\alpha = \frac{\Delta t}{\mathrm{Re}(\Delta x)^2}$ from the diffusive term and $\beta = \frac{a\Delta t}{\Delta x}$ from the convective one. A possibility is therefore to choose Δt as a constant times the minimum of these two restrictors, *i.e.*

$$\Delta t = C \min\left\{ \frac{\Delta x}{a}, \mathrm{Re}(\Delta x)^2 \right\} . \tag{29}$$

Another approach is to perform stability analysis on a linearized version of the scheme, and transfer the knowledge to the application of the nonlinear method. It has been shown that the general form of the dependency of Δt on Δx, a and Re is predicted only somewhat correctly from this type of procedure[21].

Since no thorough analysis is possible, we have chosen to do a numerical trial-and-error experiment to find the maximum time step Δt_m which produces stable results for a series of different Reynolds numbers and grid sizes. We can then choose the time step in a manner which ensures that $\Delta t < \Delta t_m$.

If the system converges to steady-state behaviour, the change in the primitive variables will approach zero. We therefore set a tolerance ϵ and advance the system in time until the relative change in the uniform norm of the vector of discrete velocity values becomes smaller than that tolerance. In other words, we require $\frac{||\mathbf{u}^{n+1}-\mathbf{u}^n||_\infty}{||\mathbf{u}^{n+1}||_\infty} < \epsilon$ for convergence.

2.1.6. Vorticity and stream function formulation

Our reference solutions are those of Ghia *et al.* [16], but their calculations are based on a vorticity and stream function formulation of the 2D Navier-Stokes equations. In order to compare our results more efficiently, we therefore compute these quantities at the end of the simulation. The scalar stream function ψ is defined for incompressible flow in 2D through the velocity components such that

$$u = \partial_y \psi \,, \quad v = -\partial_x \psi \,. \tag{30}$$

The difference between the stream function at two points equals the volumetric flux through a line contacting these points. Contour lines of the stream function are known as stream lines. Stream lines are parallel to the velocity field at all points in the domain, and trace the movement of particles in the fluid. Vorticity, on the other hand, describes the local spinning motion of the fluid at a point. Although a vector quantity in general (the curl of the velocity field), in 2D there is only one non-zero component. We thus define the vorticity as

$$\omega = |\nabla \times \boldsymbol{u}| = \partial_x v - \partial_y u \,, \tag{31}$$

which means that computation of the vorticity at grid points $(x_{i+\frac{1}{2}}, y_{j+\frac{1}{2}})$ in our mesh is straightforward given the velocity components. Insertion of Eq. (30) into Eq. (31) gives a simple Poisson equation relating ψ to ω:

$$\omega = -\nabla^2 \psi \tag{32}$$

Conversion from primitive variables to stream function and vorticity can thus be achieved by first calculating the vorticity at $(N-1)^2$ points, and subsequently solving Eq. (32) with zero boundary conditions.

2.2. Bingham plastic fluid

Extension of the 2D Navier-Stokes solver to the particular case of Non-Newtonian fluids known as Bingham plastics introduces two difficulties. Firstly, the discretization of the viscous term is cumbersome. As introduced in Section 1, the viscous term $\nabla^2 \boldsymbol{u}$ is replaced by $\nabla \cdot \boldsymbol{\tau}$ for these fluids, where

$$\boldsymbol{\tau} = \eta(\dot{\gamma})\dot{\boldsymbol{\gamma}} = \left(\frac{B}{\dot{\gamma}} + 1 \right) \dot{\boldsymbol{\gamma}} \,. \tag{33}$$

It is not possible to discretize this term implicitly in time while retaining the linearity of the system for $\tilde{\boldsymbol{u}}^{n+1}$. Secondly, the singularity of the apparent viscosity for $\dot{\gamma} = 0$ cannot be handled directly computationally.

2.2.1. Creeping flow

An idea for circumventing the first of these problems is to discretize the fluid strain rate tensor implicitly while accepting an explicit temporal discretization for the strain rate magnitude in the apparent viscosity, in other words pursuing a discretization such as $\boldsymbol{\tau}^{n+\frac{1}{2}} = \eta(\dot{\gamma}^n)\dot{\boldsymbol{\gamma}}^{n+1}$. This would result in a solvable system of equations. As we restrict ourselves to the case of creeping flows (Re = 0), however, this problem vanishes automatically. Equation (7) applied to the case of Bingham plastic fluids reads

$$\mathrm{Re}\left(\partial_t \boldsymbol{u} + \boldsymbol{u}\cdot\nabla\boldsymbol{u}\right) = -\nabla p + \nabla\cdot\eta(\dot{\gamma})\dot{\boldsymbol{\gamma}}\,, \qquad (34)$$

but when Re $\to$ 0, the left side of the equation vanishes and we are left with the problem of solving

$$\nabla p = \nabla\cdot\eta(\dot{\gamma})\dot{\boldsymbol{\gamma}} \qquad (35)$$

under the incompressibility criterion of Eq. (4). We therefore only make a note that computational solutions exist for Bingham plastics in the unsteady case (see *e.g.* Vola *et al.* [22]), and concentrate our efforts on the steady-state case when Eq. (35) is satisfied.

2.2.2. Regularization

- Treatment of singularity in effective viscosity: regularization [23]. Physical interpretation: replace "solid" in unyielded zone by high-viscostiy fluid.

$$\eta = \frac{B}{\dot{\gamma}}\left(1 - e^{-m\dot{\gamma}}\right) + 1 \qquad (36)$$

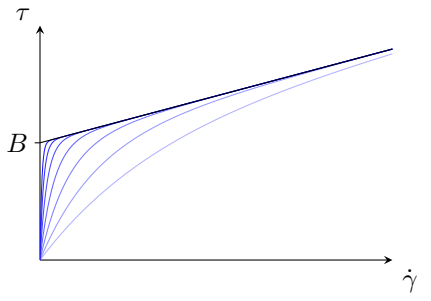

Figure 4: Regularization technique to mimic the behaviour of Bingham "plastic" plastics.

2.2.3. Spatial discretization

- Finite volume method w/o need for staggered grid, discretization of viscous term

2.2.4. SIMPLE and friends

- Solution of steady-state system: SIMPLE and its extensions

3. Results

3.1. Analysis of time step size

Text about Figure 5. We use $\Delta t = 500\Delta x/\mathrm{Re}$ based on the results. This produces stable simulations up to $N = 129$ and Re = 1000. For Re> 1000, we use $\Delta t = 100\Delta x/\mathrm{Re}$.

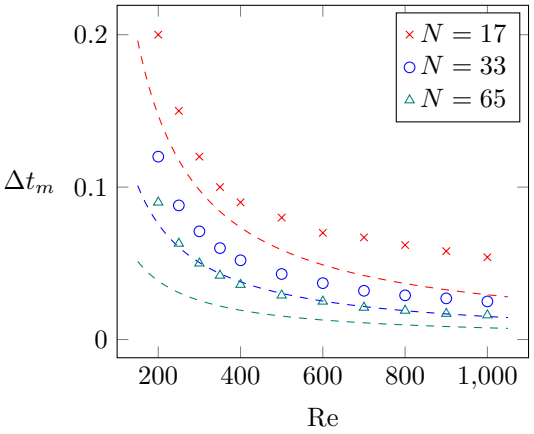

Figure 5: Time step analysi yo!

3.2. Transient behaviour

- Impulsively started
- What happens as a function of time?
- Results for different Re?

3.3. Steady-state solution

3.4. Computational efficiency

- Computational complexity of the linear systems
- Runtime (and no of time steps) as a function of Re and N

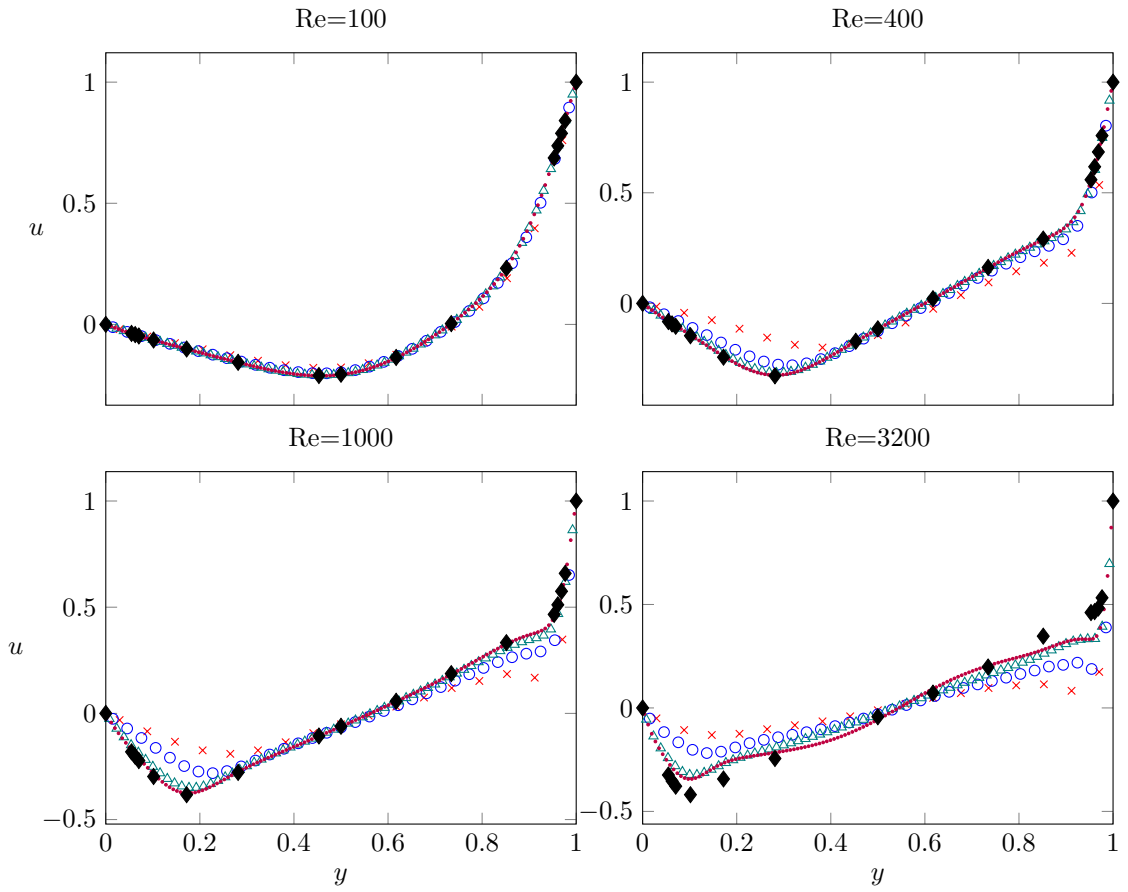

Figure 6: First component of velocity through $x = 0.5$.

4. Discussion

- Everything works, results exactly as in literature
- Transient method is slow for high Re, SIMPLE could be better
- Other improvements include Hockney algorithm and multigrid methods
- Discuss stability and computational efficiency of

5. Conclusions

References

[1] J. Marshall, A. Adcroft, C. Hill, L. Perelman, C. Heisey, A finite-volume, incompressible Navier-Stokes model for studies of the ocean on parallel computers, Journal of Geophysical Research: Oceans 102 (C3) (1997) 5753–5766.

[2] F. X. Giraldo, M. Restelli, A study of spectral element and discontinuous Galerkin methods for the Navier-Stokes equations in nonhydrostatic mesoscale atmospheric modeling: Equation sets and test cases, Journal of Computational Physics 227 (8) (2008) 3849–3877.

[3] M. M. Rai, Navier-Stokes simulations of rotor/stator interaction using patched and overlaid grids, Journal of Propulsion and Power 3 (5) (1987) 387–396.

[4] J. L. Thomas, W. K. Anderson, S. T. Krist, Navier-Stokes computations of vortical flows over low-aspect-ratio wings, AIAA journal 28 (2) (1990) 205–212.

[5] A. Jameson, L. Martinelli, N. Pierce, Optimum aerodynamic design using the Navier-Stokes equations, Theoretical and Computational Fluid Dynamics 10 (1-4) (1998) 213–237.

[6] C. S. Peskin, Numerical analysis of blood flow in the heart, Journal of Computational Physics 25 (3) (1977) 220–252.

[7] M. Mihaescu, S. Murugappan, M. Kalra, S. Khosla, E. Gutmark, Large eddy simulation and Reynolds-averaged Navier-Stokes modeling of flow in a realistic pharyngeal airway model: An investigation of obstructive sleep apnea, Journal of Biomechanics 41 (10) (2008) 2279–2288.

[8] J. Deiber, W. Schowalter, Flow through tubes with si-

nusoidal axial variations in diameter, AIChE Journal 25 (4) (1979) 638–645.
[9] G. Vinay, A. Wachs, J.-F. Agassant, Numerical simulation of weakly compressible Bingham flows: the restart of pipeline flows of waxy crude oils, Journal of non-newtonian fluid mechanics 136 (2) (2006) 93–105.
[10] M. B. Cardenas, D. T. Slottke, R. A. Ketcham, J. M. Sharp, Navier-Stokes flow and transport simulations using real fractures shows heavy tailing due to eddies, Geophysical Research Letters 34 (14).
[11] F. Boyer, C. Lapuerta, S. Minjeaud, B. Piar, M. Quintard, Cahn–Hilliard/Navier–Stokes model for the simulation of three-phase flows, Transport in Porous Media 82 (3) (2010) 463–483.
[12] C. L. M. H. Navier, Memoire sur les lois du mouvement des fluides, Mémoires de l'Académie Royale des Sciences de l'Institut de France 6 (1822) 389–440.
[13] G. G. Stokes, On the theories of the internal friction of fluids in motion and of the equilibrium and motion of elastic solids, Transactions of the Cambridge Philosophical Society 8 (1845) 287–319.
[14] C. L. Fefferman, Existence and smoothness of the Navier-Stokes equation, The Millennium Prize Problems (2006) 57–67.
[15] E. C. Bingham, An investigation of the laws of plastic flow, Bulletin of the Bureau of Standards 13 (2) (1916) 309–353.
[16] U. Ghia, K. N. Ghia, C. Shin, High-Re solutions for incompressible flow using the Navier-Stokes equations and a multigrid method, Journal of computational physics 48 (3) (1982) 387–411.
[17] O. Zikanov, Essential Computational Fluid Dynamics, John Wiley & Sons, 2010.
[18] A. J. Chorin, Numerical solution of the Navier-Stokes equations, Mathematics of Computation 22 (104) (1968) 745–762.
[19] J.-G. Liu, Projection method I: convergence and numerical boundary layers, SIAM journal on numerical analysis 32 (4) (1995) 1017–1057.
[20] G. Guennebaud, B. Jacob, et al., Eigen v3, http://eigen.tuxfamily.org (2010).
[21] W. Kress, P. Lötstedt, Time step restrictions using semi-explicit methods for the incompressible Navier–Stokes equations, Computer Methods in Applied Mechanics and Engineering 195 (33) (2006) 4433–4447.
[22] D. Vola, L. Boscardin, J. Latché, Laminar unsteady flows of Bingham fluids: a numerical strategy and some benchmark results, Journal of Computational Physics 187 (2) (2003) 441–456.
[23] T. C. Papanastasiou, Flows of materials with yield, Journal of Rheology 31 (5) (1987) 385–404.